Landslides (2012) 9:457–474
DOI 10.1007/s10346-011-0300-x
Received: 12 January 2010
Accepted: 21 September 2011
Published online: 7 December 2011


Maneesha V. Ramesh · Nirmala Vasudevan

# The Deployment of Deep-earth Sensor Probes for Landslide Detection

**Abstract** In this paper, we present a state-of-the-art wireless sensor network (WSN) of deep-earth probes (DEPs) that has been deployed to monitor an active landslide in the Western Ghats mountain range of South India. While India has one of the highest incidences of landslides and landslide-induced fatalities—primarily in the Himalayas of North India and in the Western Ghats of Central and South India—our study is perhaps the first comprehensive attempt to instrumentally detect landslides in the Western Ghats. Wireless networks have enabled us, since June 2009, to continuously monitor the deployment site in real time and from anywhere around the globe. There have been a few earlier landslide monitoring WSNs using accelerometers in Emilia Romagna Apennines, Italy; global navigation satellite system (GNSS) sensors to monitor the Hornbergl landslide, Austria; and vibrating wire stress sensors to monitor a slope in China. We improved upon these WSN systems by incorporating a variety of sensors—piezometers, dielectric moisture sensors, strain gauges, tiltmeters, a geophone, and a weather station—and installing some of these sensors as deep as 20 m below the ground surface. We present the salient aspects of the field deployment of DEPs: the selection of sensors and their incorporation in DEPs, the methodology we used in embedding these DEPs into the soil, and a few of the key aspects of the wireless sensor network. We also present a description of the deployment site and some of the results of geotechnical investigations carried out on borehole corings. Finally, we present the more interesting field data collected from the monitoring system during a rainy season in July and August 2009.

**Keywords** Landslides · Wireless sensor networks (WSNs) · Deep-earth probes (DEPs) · Western Ghats of India · Field instrumentation · Disaster monitoring

## Introduction

Landslides pose a serious hazard in many regions of the world (Nadim et al. 2006). Recent literature refers to several locations of landslide hazard-monitoring systems such as the Canelles Reservoir, Spain (Pinyol et al. 2011); the Slano Blato landslide and the Rebrnice landslide, both in Slovenia (Petkovšek et al. 2011); NW Bohemia (Vařilová et al. 2011); the Åknes rockslide, Norway (Grøneng et al. 2011); the Basilicata Region, Italy (Di Maio and Vassallo 2011); the Jiweishan Hill area, Chongqing, China (Yin et al. 2011); and Turtle Mountain, Canada (Read et al. 2005). Some of these monitoring systems have wireless data transmission, but none of them are wireless sensor network (WSN) based. In contrast, in this paper, we present an enhanced landslide monitoring system based on a wireless sensor network.

Wireless sensor networks, consisting of sensor nodes that are capable of data acquisition, data storage, data processing, and wireless data transmission, are rapidly emerging as valuable tools for monitoring environmental phenomena and are particularly suited for landslide monitoring. The sensor nodes are also capable of communicating with other nodes in the network and making decisions on the basis of these communications. Thus, a WSN provides a relatively inexpensive and reliable method to collect data on rainfall, soil pore water pressure, moisture content, and soil movement. The collected data can be subjected in real time to simple processing operations such as data aggregation, data reduction, distributed analysis, and consensus within the network itself. The processed data can then be transmitted rapidly over long distances and inhospitable terrains. Data processing reduces the amount of transmitted data and thereby reduces the power consumption of the network and increases the lifetime of the network. Furthermore, in a WSN, the data collection rate can be altered remotely or by the network taking suitable decisions itself. Thus, in a landslide monitoring WSN, data collection and transmission can be minimized during dry seasons, while all relevant sensor data can be captured and transmitted during periods of heavy rainfall. WSNs also have other attractive features such as self-organizing and self-healing capabilities, high fault tolerance, and easy integration with web-based technologies.

There are some studies on the use of WSNs for landslide monitoring. Sheth et al. (2005, 2007), the authors of SENSLIDE, proposed a WSN of strain gauges deployed at low depths (25–30 cm) and implemented this design on a laboratory test bed. Terzis et al. (2006) proposed the use of a grid of sensor columns to detect the formation of a slip surface that precedes a landslide occurrence. They tested their ideas using computer simulations. Jamaludin et al. (2006) proposed a WSN of soil temperature and slope inclination sensors to monitor slope stability. Garich (2007) designed a wireless sensor node incorporating a soil moisture and tilt sensor. Kim (2008) developed a wireless sensor node to measure the inclination angle and acceleration of a hill slope. The nodes were tested on a small slope equipped with an artificial rainfall simulator. It was found that these sensor nodes can detect ground motion once the slope begins to move. Other comprehensive studies on the use of WSNs for landslide detection include SLEWS (Arnhardt et al. 2007, 2009, 2010; Fernández-Steeger et al. 2009) and the work of Lee (2009). In addition, Fang et al. (2008), Hloupis et al. (2010), and Tang and Dai (2010) discussed the application of wireless sensor technology to landslide detection.

To our knowledge, there are only three published accounts describing the actual implementation of a WSN-based landslide monitoring system. Rosi et al. (2007) described a field deployment of accelerometers in Emilia Romagna Apennines, Italy. Glabsch et al. (2009) deployed a WSN to monitor the Hornbergl landslide, Austria. Their network consists of two sensor nodes, each equipped with a global navigation satellite system (GNSS) sensor. Xinjian et al. (2010) deployed a network of vibrating wire stress sensors to monitor bolt stress on a slope in China. Finally, internet searches reveal that there may be WSN-based field deployments of soil moisture sensors, rain gauges, and inclinometers in Malaysia (Universiti Putra Malaysia) and of movement sensors in Idaho,

USA (by a team at the Southwest Research Institute, San Antonio, Texas).

In this project, which was initiated in September 2006 (Ramesh et al. 2007; Ramesh 2009), we deployed a wireless sensor network of 20 deep-earth probes (DEPs) to monitor a landslide in South India. Each deep-earth probe consists of a variety of sensors—piezometers, strain gauges, tiltmeters, dielectric moisture sensors, and geophones—and some of these sensors were installed as deep as 20 m below the ground surface. The sensors were interfaced to motes (miniature data processing and wireless transmission devices) to form wireless sensor nodes. Data collected by the sensor nodes are transmitted through a heterogeneous network (described in this paper) to our university campus over an aerial distance of 130 km, and the received data are then streamed live to the internet. The use of a heterogeneous network enables us to transmit data over long distances. The long distance transmission and subsequent real-time streaming of sensor data are some of the attractions of this system—it is these features that enable us to monitor a remote site in real time from anywhere in the world and to issue timely warnings as needed.

In addition to the successful implementation of a WSN for landslide monitoring, this study has other features of interest. We followed some of the newer methods in the deployment of piezometers and soil-strain probes. We deployed nests of five to eight removable piezometers in fully grouted boreholes as suggested in more recent literature (Contreras et al. 2008; Mikkelsen and Green 2003; McKenna 1995). Furthermore, we designed soil-strain probes as described by Ochiai et al. (2004). Similar probes were used by Williams (1957), Barr and Swanston (1970), Yamada and Kurashige (1996), and many others. However, in the literature, strain gauges are affixed on casings (or strips) that vary in length from 50 cm–2 m. Our casings vary in length from 10–21 m, and the strain gauges can measure movement as deep as 20 m. We have been collecting sensor data from the field deployment since March 2008. Some sensor data (particularly sensor data from strain gauges deployed at depths of 10.75 m) show interesting variations during periods of heavy rainfall as shown in this paper.

Landslides in India occur primarily in the Himalayan mountain ranges (Tahir and Ha 2011; Sattar et al. 2011) and in the Western Ghats mountain ranges (Kuriakose et al. 2009). Despite the fact that India has one of the highest incidences of landslides and landslide-induced fatalities (Kirschbaum et al. 2010), there are only a few studies on landslide instrumentation in the Western Ghats (e.g., Kuriakose et al. 2008). This is perhaps the first comprehensive study on field instrumentation in the landslide-prone Western Ghats.

### The deployment site—Anthoniar Colony, Munnar

The deployment site—Anthoniar Colony hill (Fig. 1)—is located on a 7-acre area, approximately 700 m northwest of the tourist town Munnar in the Idduki District of Kerala State, South India (Fig. 2). Munnar lies on the landslide-prone Western Ghats mountain range (Fig. 3), and the region in and around Munnar varies in height from 2,000–2,600 m above sea level. The temperature ranges from 10–25°C; occasionally in the month of January, it drops as low as 0°C. The region typically receives

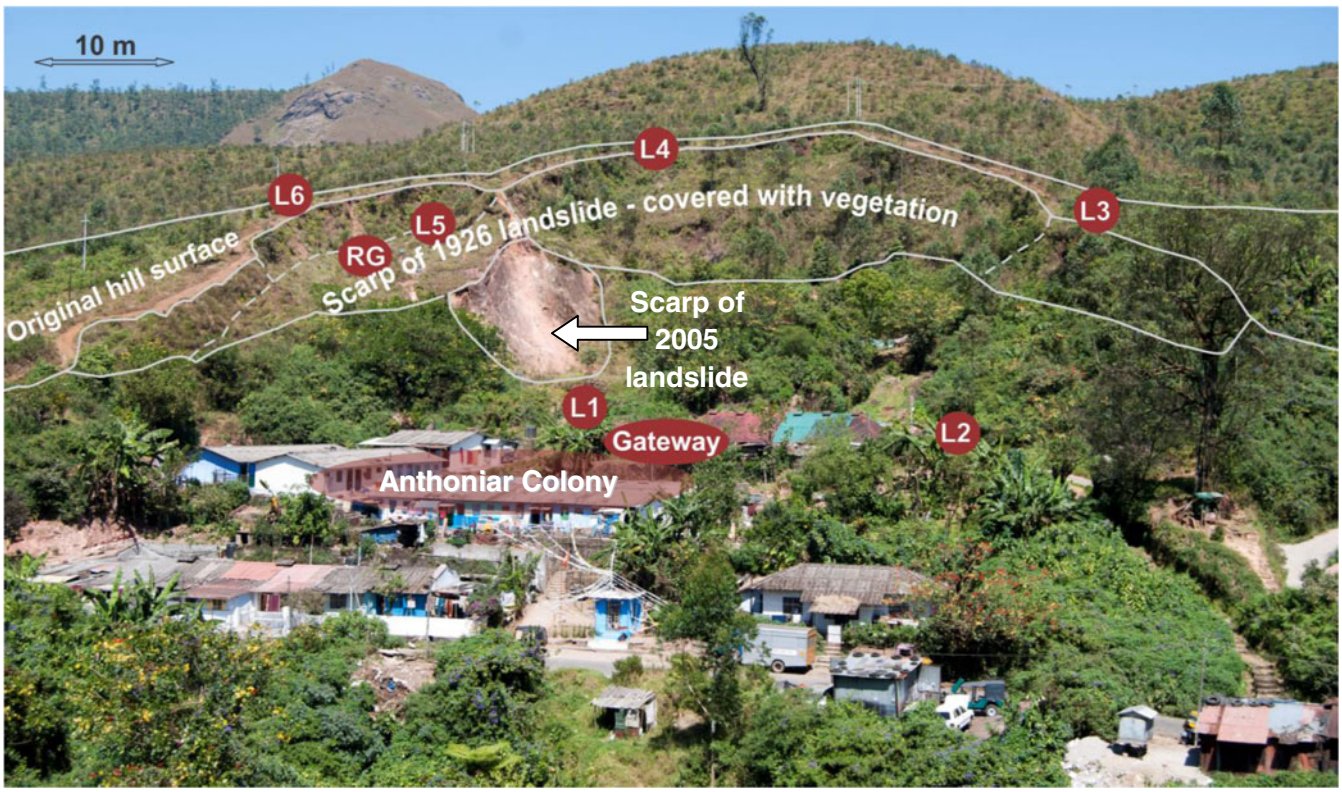


**Fig. 1** Deployment site—Anthoniar Colony, Munnar, Kerala, South India. *L1*, *L2*… refer to the locations of the deep-earth probes (DEPs), and *RG* refers to the location of the rain gauge. The gateway of the wireless sensor network (WSN) is also indicated

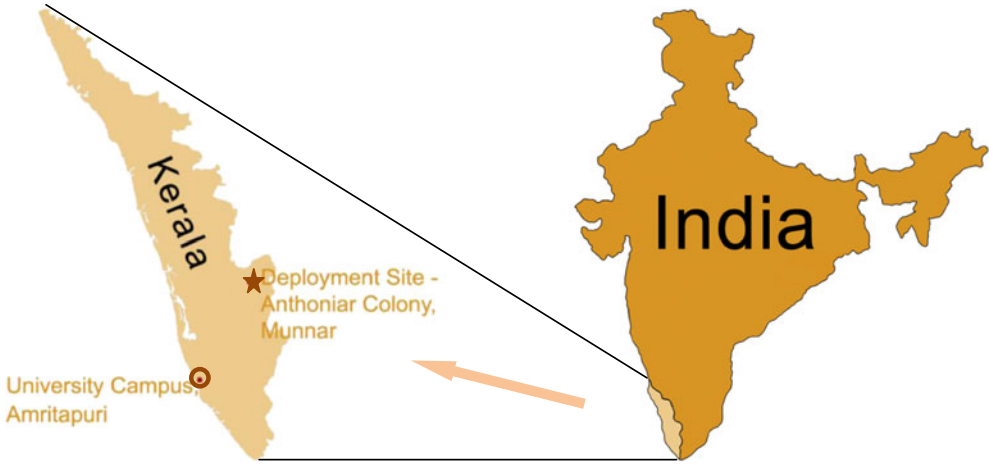


**Fig. 2** Kerala State in southwest India. Munnar town in Kerala. The deployment site—Anthoniar Colony—is 700 m northwest of Munnar. Sensor data are transmitted from Anthoniar Colony to the university campus over an aerial distance of 130 km

3,500–5,500 mm rainfall every year. The main monsoon season lasts from June to September and usually results in 2,500–4,500 mm of rain. These monsoons are caused by moisture-laden winds from the Indian Ocean and are known as the southwest monsoons. The southwest monsoons are almost immediately followed by the northeast monsoons in October and November, which result in approximately 500 mm of rain. Maximum rainfall typically occurs in July.

The soil at the deployment site is basically lateritic soil overlying bedrock of granite gneiss. The predominant clay mineral is kaolinite. The soil cover extends to a depth of 15–18 m at the toe of the hill, while it is over 30 m deep in the higher regions of the hill. Soil samples extracted from a borehole drilled at the toe of the hill were subjected to various geotechnical tests, performed in accordance with the Indian standard. Some of the test results are summarized in Table 1.

Anthoniar Colony was chosen as the deployment site on the basis of many considerations:

1. Several rainfall-induced landslides have occurred in the vicinity of this location.
2. Two earlier rainfall-triggered landslides occurred at this exact location. The first one occurred in 1926. It was a massive landslide with an estimated volume of $10^5$ $m^3$. Debris from the landslide covered a considerable portion of the present-day Munnar town. However, no one was living in this region at that time, and there were no causalities. Laborers would come daily to work in tea plantations around this

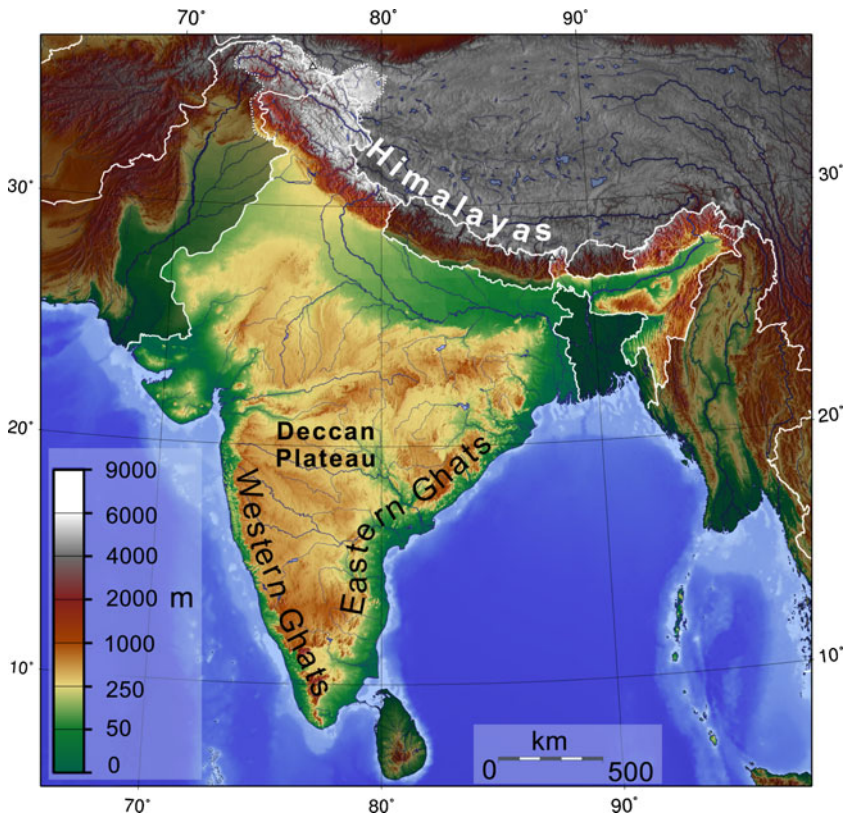


**Fig. 3** The Western Ghats mountain range along the western coast of India

**Table 1** Summary of geotechnical properties of lateritic soil samples from the deployment site

| Property | Value |
|---|---|
| Clay size fraction (particle size <2 μm) | Average for all tested samples, 15% |
| Plasticity index | Average for all tested samples, 23 |
| Specific gravity | ~2.57 |
| Bulk density | Average for all tested samples, 19.2 kN/m$^3$ |
| Natural moisture content of saturated sample | Average for all tested samples, 22% |
| Permeability of saturated sample | $10^{-5}$–$10^{-6}$ cm/s |
| Cohesion of saturated sample (as measured in consolidated–drained direct shear tests) | $10^{-1}$ kg/cm$^2$ |
| Angle of internal friction of saturated sample (as measured in consolidated–drained direct shear tests) | Approximate range of values, 27–35° |

region, and they photographed the slide after its occurrence. The scarp of this slide is visible even today although it is covered with vegetation. The scarp has a concave curvature. The second landslide occurred on 26 July 2005. It was a complex rotational slide–debris flow with a volume of approximately $10^4$ m$^3$ and was triggered by a torrential downpour. The total rainfall recorded in Munnar on 26 July 2005 was 451 mm. The same downpour also triggered two other landslides in the vicinity of Munnar—one at the Government Arts and Science College, 1.4 km southeast of Munnar and the other at the Subrahmaniam Temple on the outskirts of Munnar town. The landslides resulted in eight deaths.

3. We feel that there is a strong likelihood of further landslides at this location for many reasons which include the following:

   (a) The toe of the hill was cut during the construction of homes and roads.
   (b) There are fissures along the hill.
   (c) The soil at the toe of the hill remains almost fully saturated (degree of saturation $S$ >87%) for most of the year—the soil is moist, and constant seepage flow is observed even during the dry season.
   (d) The soil in this region has an apparent cohesion when it is partially saturated. However, rainwater infiltration results in a loss of this apparent cohesion and adversely affects slope stability.
   (e) There are large deposits of quartz on the surface layer of the soil which allow water to infiltrate and saturate the subsurface soil layers.
   (f) There are deposits of red expansive clay (activity 2.19) in regions of the hill. The expansive action of these clays can potentially destabilize the hill and cause a landslide.

4. Landslides that occur could be massive because the soil thickness is more than 20 m.
5. Landslide activity could be fatal because there are people living at the foot of the hill.
6. From a data transmission perspective, the cellular network and broadband connectivity are good. In the event of no satellite connectivity, these networks can serve as an alternative for data transmission.
7. Finally, the site is accessible by road, and equipment can be transported to the site with comparative ease.

We identified six locations on the site as ideal for the deployment of field instrumentation. We labeled them as *L1*, *L2*, *L3*, *L4*, *L5*, and *L6* (Figs. 1 and 4). We briefly describe these locations and also provide rough estimates of the water table depths at these locations (Table 2). These water table depths were measured during the months of January–March, when there is very little rainfall.

*L1*: a location near the toe of the 2005 landslide
- There is substantial pore water pressure underneath the ground at this location.
- Constant seepage flow is observed at this location.
- A considerable amount of debris from the 2005 landslide was deposited at this location. The landslide actually resulted in four fatalities very close to this location.

*L2*: another location in the lower regions of the hill
- There is substantial pore water pressure underneath the ground at this location also.
- Constant seepage flow is observed near this location.

*L3*, *L5*: locations in the middle region of the hill
- Creep movements are evident at these locations.

*L4*: a location near the crown of the hill
- Creep movements are evident at this location.

*L6*: a relatively stable location in the upper regions of the hill. Sensors deployed at *L6* can be used to compare the responses of sensors in unstable positions with those of sensors in relatively stable positions. Also, we anticipate that the deployment at *L6* will give insight as to the distance from which sensors can detect landslide-associated phenomena.

Deep-earth probes were installed at all six locations. The installation was completed in two phases—a pilot deployment of 3 DEPs in March 2008 followed by a full-scale deployment of 17 DEPs (6 January 2009–10 March 2009).

## Deployment of deep-earth probes

### Wireless deep-earth probe

The concept of a wireless deep-earth probe has its origin in the work of Terzis et al. (2006). In this paper, we use the term "deep-earth probe" (DEP) to refer to a combination of sensors or probes that are embedded as a single unit in a hole drilled into the earth's surface. DEPs contain sensors that are appropriate for landslide monitoring, such as piezometers, tensiometers, inclinometers, etc. As in any landslide-monitor-

**Fig. 4** Contour map of the deployment site. The grid intervals are 10 m×10 m, and the contour intervals are 1 m. *L1*, *L2*… refer to the deep-earth probe locations. *L1* lies near the toe of the 2005 landslide; *L4* lies near the crown of the hill; and *L5* lies just above the main scarp of the 2005 landslide. A few of the relay nodes (*R*), the gateway, and the Field Management Center (FMC) of the wireless sensor network are also indicated on the map

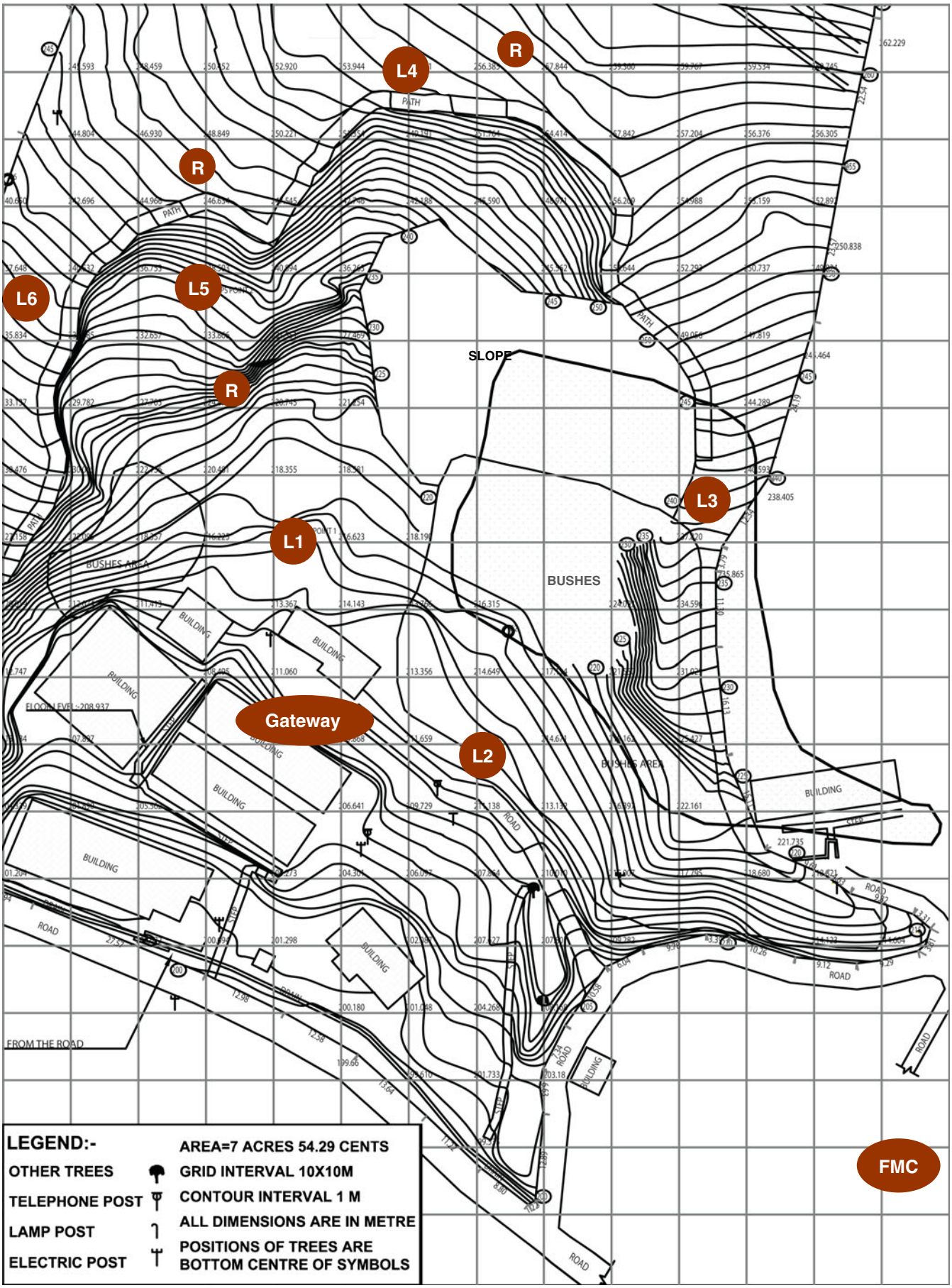
L4
R
R
L6
L5
R
SLOPE
L3
L1
BUSHES AREA
BUSHES
BUILDING
Gateway
L2
BUSHES AREA
ROAD
FROM THE ROAD
FMC
LEGEND:-
OTHER TREES
TELEPHONE POST
LAMP POST
ELECTRIC POST
AREA=7 ACRES 54.29 CENTS
GRID INTERVAL 10X10M
CONTOUR INTERVAL 1 M
ALL DIMENSIONS ARE IN METRE
POSITIONS OF TREES ARE BOTTOM CENTRE OF SYMBOLS

**Table 2** Water table depths at locations *L1–L6*

| Location | Dry season water table depth (m) |
|---|---|
| L1 | 2.1 |
| L2 | 3.4 |
| L3 | 15.0 |
| L4 | 16.5 |
| L5 | 12.8 |
| L6 | 15.8 |

ing scenario, the choice of sensors (number, type, and placement) depends on the local geology and the subsurface conditions at the position of the DEP. As a result, each DEP is unique in its design.

All the sensors in the DEP are interfaced to a miniature data processing and wireless transmission device, referred to as a "mote" in wireless sensor node terminology, via a data acquisition (DAQ) board to form a wireless deep-earth probe. Thus, a wireless deep-earth probe can collect sensor data, process it, and then transmit it wirelessly. Wireless DEPs can also communicate with other wireless DEPs in the network and make decisions based on these communications. A schematic representation of a wireless DEP is shown in Fig. 5; an actual DEP may consist of different sensors than those shown in the figure.

### Selection of sensors

WSNs call for low-cost sensors that easily can be deployed en masse over a wide area. So, we explored the use of inexpensive and easy-to-deploy instrumentation such as dielectric moisture sensors, strain gauges, and tiltmeters (in lieu of costlier inclinometers). Anthoniar Colony is prone to rainfall-induced landslides, so piezometers were included in the DEPs at all six locations. The DEPs in the Anthoniar Colony pilot and full-scale deployments include the following:

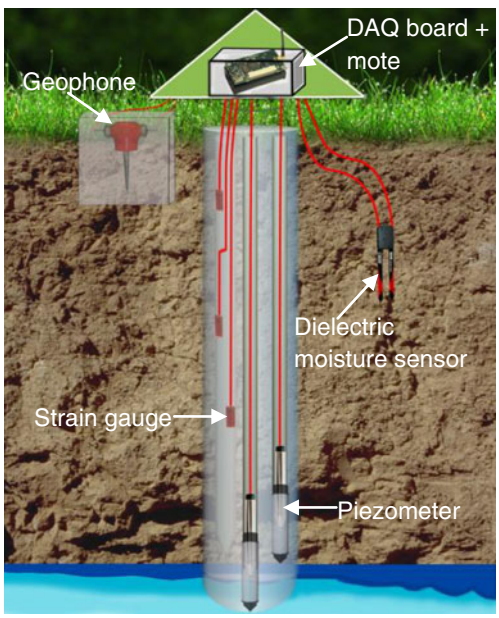


**Fig. 5** Schematic diagram of a wireless DEP

#### Piezometers

Strain gauge-based piezometers were chosen as they can be interfaced more easily with the wireless network than vibrating wire piezometers. Moreover, current-based (rather than voltage-based) 4–20 mA output piezometers were selected to avoid errors due to wire length. Also, while the piezometers of the pilot deployment are permanently installed, removable piezometers were chosen during the full-scale deployment. Thus, most of the piezometers can be easily removed for periodic recalibration, troubleshooting, or replacement as needed.

#### Dielectric moisture sensors (DMSs)

DMSs were installed to measure the volumetric water content of the soil. Soil moisture content is closely related to groundwater infiltration and the subsequent changes in soil pore water pressure. Related quantities such as wetness index are widely used in slope stability analysis (Rosso et al. 2006; Acharya et al. 2006; De Vleeschauwer and De Smedt 2002; Van Westen and Terlien 1996; Montgomery and Dietrich 1994). Predictably, moisture sensors are used in both landslide laboratory experiments (Huang et al. 2008; Tohari et al. 2007; Orense et al. 2004; Shimoma et al. 2002) and in field deployments (Matsushi and Matsukura 2007; Ray and Jacobs 2007; Baum et al. 2005).

We included dielectric moisture sensors (Fig. 6) in many of the DEPs to explore their potential as inexpensive landslide-monitoring devices. Our intention was to obtain data on the degree of saturation of the soil from these sensors and establish a quantitative relationship between DMS readings and rainwater infiltration rate, which is an important parameter in models of rainfall-triggered landslides (e.g., Iverson 2000).

#### Strain gauges

Strain gauges were included in the DEPs to detect slope movement. Strain gauges were affixed to the outer surface of 3-m long ABS plastic inclinometer casings (as shown in Figs. 7 and 8), and several inclinometer casings were connected to one another to form one long casing (Fig. 9). We deployed only one such casing during the pilot deployment, and it was 6 m long (Fig. 9) with 5 m below the ground surface. We deployed six more casings during the full-scale deployment, and they varied in length with 10–21 m of casing below the ground surface. The strain gauges, themselves, were oriented along the vertical axis of these casings, and they indicate any bending of the casing caused by ground movements (Fig. 7a). The actual positions of the strain gauges on the casing were determined on the basis of the soil profile, observed creep movements, and the likelihood of future creep movements at that

**Fig. 6** Dielectric moisture sensor (DMS) to measure the volumetric water content of the soil. The probes are inserted completely into the soil

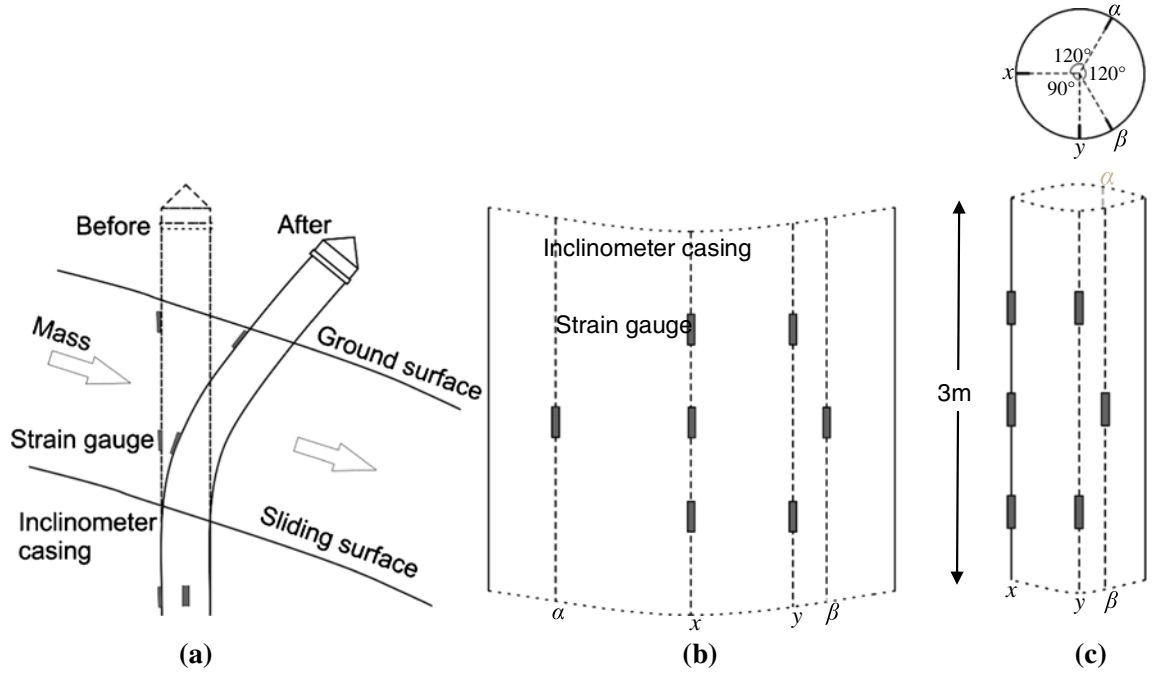


**Fig. 7** **a** Detection of slope movement using strain gauges. **b**, **c** As explained in the paper, strain gauges have been installed to detect movement in one of four possible directions: $x$, $y$, $\alpha$, and $\beta$. The $y$-direction is 90° from the $x$-direction, either in the anti-clockwise direction as shown in the figures or in the clockwise direction. In **c**, we show an inclinometer casing, while in **b**, the same cylindrical inclinometer casing is mapped onto a rectangle. Explaining the notation used in this paper, if we assume that **b** depicts strain gauges deployed at depths of 10, 10.75, and 11.5 m, we would write 10 m($x$), 10 m($y$), 10.75 m($\alpha$), 10.75 m($x$), 10.75 m($\beta$), 11.5 m($x$), and 11.5 m($y$)

particular DEP location. The strain gauges were installed to detect movement in four possible directions (Fig. 7b, c):

(a) In the down-slope $x$-direction (the direction along which the slope is most likely to fail);
(b) The $y$-direction, which is perpendicular to the $x$-direction, either in the clockwise direction or in the anti-clockwise direction, in whichever of the two directions the slope is more likely to fail;
(c) The $\alpha$-direction which is 120° from the $x$-direction in the clockwise direction (when viewed from the top of the casing); and
(d) The $\beta$-direction which is 120° from the $x$-direction in the anti-clockwise direction (when viewed from the top of the casing).

Laboratory tests are being conducted to correlate slope movements and the corresponding bending of the casing with strain gauge readings.

The resistances of the wires connecting the strain gauges to the interfacing circuitry (DAQ board) are fairly independent of temperature. These wires were run inside heat shrink tubing for added protection. The strain gauges were sealed with silicon and then covered with mastic tape, and all joints and holes in the casing were sealed with mastic tape and two-part epoxy. Caps were fitted on the top and bottom of the casing, and the unit was installed in a borehole using the fully grouted method.

An obvious advantage of strain gauges is that they are very inexpensive compared to inclinometers, which are more routinely used to detect landslide related earth movements.

### Tiltmeters

As mentioned earlier, we explored the use of inexpensive instruments. Consequently, in-house designed tiltmeters (in lieu of more expensive commercially available inclinometers) were inserted permanently into the inclinometer casing (Fig. 9) of the pilot deployment. Each tiltmeter measured tilt along the positive and negative axes of both the down-slope $x$-direction and the $y$-direction (perpendicular to the $x$-direction). In addition to monitoring the tilt, we intended to use these tiltmeters to calibrate the strain gauges on


**Fig. 8** Strain gauges fixed on an inclinometer casing


**Fig. 9** Strain gauges on an inclinometer casing—ready for installation

**Table 3** Pilot deployment (March 2008) of three DEPs

| DEP # | Location | Drilling method | Sensor installation |
|---|---|---|---|
| 1 | L1 | Auger | Piezometer installed at a depth of 2.0 m using the traditional sand pack and bentonite seal method |
| | | | Geophone; installation described in this paper |
| 2 | L1 | Auger | Piezometer installed at a depth of 5.0 m using the traditional sand pack and bentonite seal method |
| | | | DMS pushed into the bottom of a 65-cm hole, which was repacked with earth |
| 3 | L5 | Auger | Strain gauges at depths of 1.5 m($x$), 2.5 m($x$), and 4.0 m($x$); installation described in this paper |
| | | | Tiltmeters at depths of 1.0, 2.0, and 3.5 m; inserted into the inclinometer casing |
| | | | DMS pushed into the bottom of a 30-cm hole, which was repacked with earth |

*DEP* deep-earth probe, *DMS dielectric moisture sensor*

the inclinometer casing. However, the tiltmeters stopped working approximately a month after their installation, presumably due to the intrusion of water into their electronic circuitry. Since the tiltmeters were permanently installed, we were not able to troubleshoot them.

We redesigned the tiltmeters and deployed them on 25 June 2011. The new tiltmeters have improved water proofing and are removable.

### Geophone

A geophone was included in a DEP at *L1* during the pilot deployment. As in a typical geophone installation for a site response study, a 60×30×30 $cm^3$ concrete pad was made with 30 cm extending below the ground, and the geophone was pushed into the wet concrete.

These sensors (piezometers, DMSs, strain gauges, tiltmeters, and geophone) were included in the deep-earth probes.

### Weather station

In addition to the wireless DEPs, a weather station was connected to the wireless network. The weather station was installed near *L5*, in the middle region of the hill (Fig. 1), and it can measure rain intensity, humidity, temperature, pressure, wind speed, and wind direction. The weather station uses a tipping bucket rain gauge to measure rainfall.

## Pilot deployment

In a pilot deployment that was completed in March 2008, two DEPs were installed at *L1*, while a third DEP was installed at *L5*. Table 3 summarizes some aspects of the pilot deployment (Ramesh 2009).

## Full-scale deployment

In the full-scale deployment (6 January 2009–10 March 2009), we installed 17 additional DEPs at far greater depths than in the pilot deployment. Each DEP contained many more sensors as well. We also introduced some changes in the drilling and installation procedures.

For instance, rather than installing piezometers during the deployment, we installed piezometer filter tips, also referred to as "filter tips" or simply "tips" (Fig. 10), which allow removable strain gauge piezometers (Fig. 11) or vibrating wire piezometers to be inserted whenever desired. Removable piezometers offer some distinct advantages over typical permanently installed piezometers. Removable piezometers can be easily installed in the filter tips, months after the installation of the tips. In the case of a sensor failure, the piezometers can be removed for troubleshooting or replacement. They can also be removed for periodic recalibration.

The piezometer filter tip is a filter unit made of a porous material that allows water to pass through it. The filter tip has a threaded end to which a PVC pipe can be attached. The filter tip (and the desired length of PVC pipe) can be inserted into a DEP borehole, and a removable piezometer can be inserted into the filter tip through the PVC pipe at a later time. The piezometer has an o-ring and heavy weights attached to it that seal the piezometer to the filter tip.

We deployed a total of 42 piezometer filter tips which were arranged in nests of 3–8 tips in 8 of the 17 DEP boreholes. The tips were installed at different depths. We placed tips both above and below the estimated dry season water table depths (Table 2) to measure both negative and positive pore pressures. In addition, we placed at least one filter tip in most of the identified soil layers. Two DEPs containing nested tips were installed at both *L1* and *L2* (as explained later), and one DEP of nested tips was installed at each of the other four locations.

We inserted piezometers into six tips between June and August 2009 and into another six in June 2010. Once all the piezometers are inserted into their corresponding tips, we intend

**Fig. 10** Piezometer filter tip

**Fig. 11** Removable strain gauge piezometer

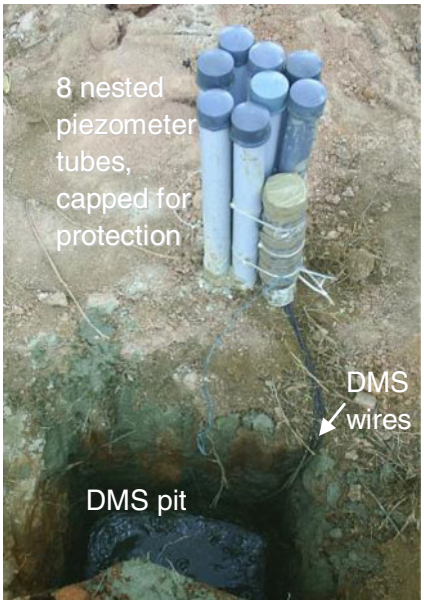


**Fig. 12** *L6* during the deployment of sensors

to study the variation of pore pressure with depth and with changes in soil strata.

All the nested filter tips were installed in fully grouted boreholes (Contreras et al. 2008; Mikkelsen and Green 2003; McKenna 1995), without using a sand pack and bentonite seal. We have performed laboratory tests comparing the performance of piezometers installed in the traditional sand pack and bentonite seal method with piezometers installed via the fully grouted method. Based on our experiences with the pilot deployment, the full-scale deployment, and the laboratory tests, we believe that both methods give comparable results, but the fully grouted method is faster, easier to install, and more fail proof.

Regarding the strain gauges, we were satisfied with the installation procedures during the pilot deployment and adopted the same installation procedures during the full-scale deployment. However, in contrast to the 5–6-m long casing installed during the pilot, during the full-scale deployment, we installed casings ranging in length from 10–21 m in separate DEPs at each of the six locations.

We inserted dielectric moisture sensors into the walls of boreholes containing either piezometer filter tips or the inclinometer casing. As the probes had to be pushed completely into the soil, it was not realistic to install them at depths greater than approximately 0.7 m in a 15–18-cm diameter borehole. Huge pits (2 m deep, 0.5 m wide, and 2 m long) were dug at *L3*, *L4*, and *L6*, and DMSs were inserted into the walls of these pits. A portion of the pit (away from the wall where the DMSs had been inserted) was refilled with earth, and the earth was compressed thoroughly. The portion of the pit near the DMSs was fully grouted with the grout used for the piezometer installation. A partially grouted DMS pit is visible in Fig. 12.

Figures 12, 13, and 14 depict DEPs at *L6*, *L4*, and *L3* respectively at different stages of the full-scale installation process. We have also included an abridged bore log of *L4* (Table 4), along with a drawing depicting the sensors at *L4* after the complete installation (Fig. 15).

During the pilot deployment, we used an auger to drill holes for the installation of DEPs. However, we wanted to obtain undisturbed soil samples while drilling. Hence, during the full-scale deployment, we used a diesel-powered rotary drilling machine (Fig. 16), and boreholes were drilled using the mud circulation technique. Furthermore, the use of a drilling machine enabled us to drill 21-m deep boreholes. As an added benefit, we could later use the drill pump to achieve the high-shear mixing required for the preparation of grout and to pump the grout into the boreholes.

With the drilling machine, it was possible to drill a hole large enough to contain all the required sensors; however, at least two boreholes (each approximately 15 cm in diameter) were drilled at each of the six locations for the following reasons:

1. From the first borehole, two 25.4-cm tubes of undisturbed soil samples were extracted for every meter drilled. The presence

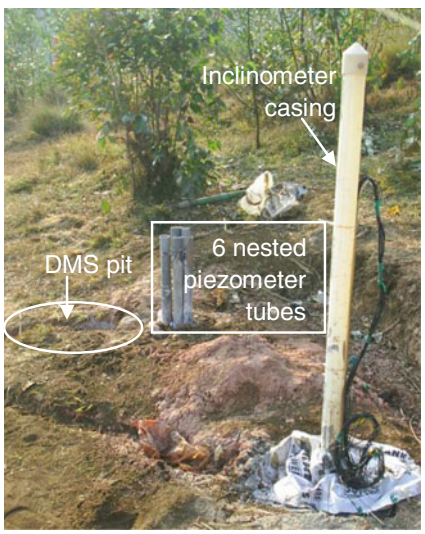


**Fig. 13** *L4*, above the ground, during the deployment of sensors


**Fig. 14** *L3* after the deployment of the sensors and the wireless sensor network. Refer to Fig. 15 for additional components

of a second borehole facilitated the standard penetration test and the extraction of a third tube of soil for each meter drilled.
2. With two closely located boreholes, it was possible to perform field permeability tests such as pumping-in and pumping-out tests.
3. The time involved in drilling a single larger hole was estimated to be nearly the same as the time involved in drilling two holes of smaller diameters.

Slurry of bentonite and mud was used as the drilling fluid. The boreholes were uncased due to the concern that the removal of such a casing at the end of the drilling operation could potentially cause the borehole to collapse. The casing had to be removed in order that the sensors can record geophysical data.

As shown in Table 5, boreholes containing piezometer filter tips were drilled deeper than the maximum water table depths at their locations. Boreholes containing the inclinometer casing were drilled significantly deeper than any observed plane of weakness. For instance, we observed a quartz sericite band at a depth of 12–13 m at *L3*. We planned to have all boreholes at a particular DEP location to be of similar depths to enable us to compare responses of different sensors installed at a comparable depth. At *L1* and *L2* (in the toe regions of the hill), weathered rock was encountered at a depth of approximately 15 m. However, due to the increased pore water pressure at *L1* and *L2*, there was an increased probability of the boreholes collapsing (both during the drilling of the boreholes and during the installation of the DEPs). Consequently, it was decided to drill shallower holes at *L1* and *L2*.

Unforeseen circumstances led to drilling several boreholes at *L1* and *L2*. At *L1*, there is considerable pore water pressure underneath the ground surface. One of the boreholes did collapse during the installation of piezometer filter tips due to this water pressure. The result was only a 3-m deep hole. A second borehole was then drilled a few meters away from the first borehole. Piezometer filter tips were installed in both boreholes. The inclinometer casing with strain gauges was installed in a third borehole at *L1*.

While drilling the second borehole at *L2* (near the residential colony at the base of the hill), a concrete structure was encountered approximately 6 m below the ground surface. Drilling had to be terminated and a new borehole was drilled a few meters away. Piezometer filter tips were installed in two boreholes, and the inclinometer casing was installed in the third borehole.

To make the grout mix used for the boreholes and pits, cement was added to a barrel of water in a fixed water:cement ratio of 2.6:1 kg (Mikkelsen and Green 2003; Contreras et al. 2008; McKenna 1995). Bentonite was added till a thick creamy mix of pancake batter consistency was obtained. The amount of bentonite required for the correct consistency varied each time the grout was made. The initial setting time of the grout mix also varied dramatically on each occasion that the grout was prepared. This variance may be due to either differences in the brand of cement or bentonite being used (the same brands of cement and bentonite were not always available at the deployment site) or differences in the weather (afternoons were extremely hot, while it was chilly in the evenings). To ensure the best results, a small quantity of test grout was always prepared immediately before the preparation of the larger quantity needed for the installation.

The drill rig pump of the drilling machine was utilized to pump grout into tremie pipes fitted in the boreholes. During the installation of the nested piezometer filter tips, special care was taken to ensure that all the tips were in contact with the surrounding grout and not enclosed by other filter tip tubes.

### Wireless sensor network

The sensors were interfaced to a data acquisition board through signal conditioning circuitry (Ramesh 2009), and, in turn, the DAQ board connects the sensors to a mote to form a wireless sensor node. The signal conditioning circuitries, DAQ boards, and

**Table 4** An excerpt from the bore log of *L4*

| Depth where soil layer begins (m) | Layer thickness (m) | Description of soil |
|---|---|---|
| 0 | 0.4 | Gravel |
| 0.4 | 1.2 | Silty lateritic clay with sand and pebbles |
| 1.6 | 7.1 | Lateritic silt (red and yellow soil grains present) |
| 8.7 | 5.5 | Lateritic clay with sand and silt (yellow, red, and white soil grains) |
| 14.2 | 2.7 | Silt and weathered rock (brown, red, yellow, and white soil grains) |
| 16.9 | – | Silty lateritic clay with sand (white and red soil grains) |

Borehole drilling terminated at a depth of 21.0 m

**Fig. 15** $L_4$, beneath the ground, after the complete deployment. The signal conditioning circuitry interfaces the sensors to a mote via a DAQ board. The power supply circuitry converts the power supplied by the batteries for use in the other circuits. Additional details are provided in the paper

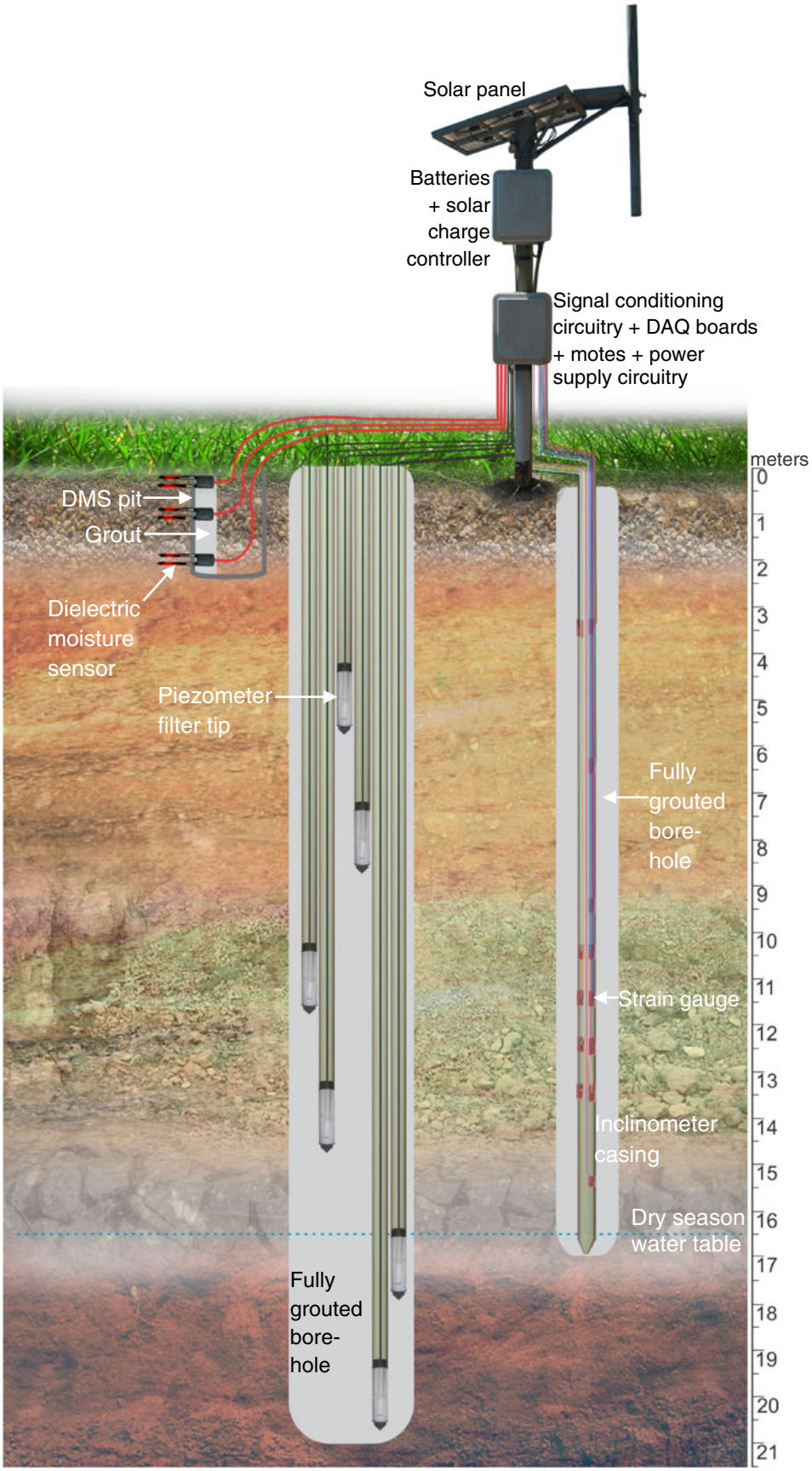

**Fig. 16** Drilling machine at *L3*

motes are all powered by lead acid batteries that store energy generated by a solar panel (Figs. 13 and 15). A solar charge controller charges the lead acid batteries and also protects the batteries from overcharging, while power supply circuitry converts the voltages from the batteries for use in the various circuits. We also installed external antennas (Fig. 13) to extend the communication range of the wireless sensor nodes.

Data collected by the sensor nodes are transmitted through a network of relay nodes to the gateway using the Institute of Electrical and Electronics Engineers (IEEE) 802.15.4/Zigbee standard (Figs. 1 and 4). The gateway is a link between two different networks and has data storage, data processing, and data transmission capabilities. In our case, the gateway is a link between the 802.15.4 network and a WiFi (802.11g) network. The data are transmitted from the gateway to a Field Management Center or FMC, a few hundred meters away, using WiFi (Fig. 4). There is a satellite link at the FMC, and data are transmitted from the FMC to the university campus, over an aerial distance of 130 km, through the satellite network (VSAT). In the event of no satellite connectivity, the cellular network or a broadband connection serves as an alternative means for data transmission. The use of a heterogeneous network (IEEE standard 802.15.4, WiFi, and VSAT) enables us to transmit data over long distances and monitor a remote site.

Although many sensors were installed at the deployment site during the full-scale deployment (January–March 2009), by the end of August 2009, only 49 sensors were connected to the wireless sensor network. Eight sensors were connected at each of the six DEP locations plus the weather station that was connected directly to the satellite network (Table 6). Ongoing work includes interfacing all (~150) deployed sensors to the corresponding motes. Data are currently being sampled every 30 s. This sampling rate can be dynamically altered; the maximum sampling rate is 20 data samples per second. Data received at the university campus are streamed live to the internet and can be viewed online through a password-protected website at www.winsoc.org.

## Results and discussion

We have been collecting sensor data intermittently from the pilot deployment since March 2008 and continuously since the full-scale deployment began operation in June 2009. Sensor data are streamed

**Table 5** Full-scale deployment (6 January 2009–10 March 2009) of 17 DEPs

| DEP # | Location | Sensor installation | Depth of borehole/pit (m) | Water table depth (m) (from Table 2) |
|---|---|---|---|---|
| 1 | L1 | Piezometers, DMSs | 3.1 | 2.1 |
| 2 | L1 | Piezometers | 15.7 | 2.1 |
| 3 | L1 | Strain gauges on inclinometer casing | 10.0 | |
| 4 | L2 | Piezometers, DMSs | 6.3 | 3.4 |
| 5 | L2 | Piezometers | 10.0 | 3.4 |
| 6 | L2 | Strain gauges on inclinometer casing, DMSs | 13.5 | |
| 7 | L3 | DMS pit | 1.0 | |
| 8 | L3 | Piezometers | 16.0 | 15.0 |
| 9 | L3 | Strain gauges on inclinometer casing | 21.0 | |
| 10 | L4 | DMS pit | 2.0 | |
| 11 | L4 | Piezometers | 21.0 | 16.5 |
| 12 | L4 | Strain gauges on inclinometer casing | 17.0 | |
| 13 | L5 | Piezometers, DMSs | 21.0 | 12.8 |
| 14 | L5 | Strain gauges on inclinometer casing | 20.5 | |
| 15 | L6 | DMS pit | 2.0 | |
| 16 | L6 | Piezometers | 20.0 | 15.8 |
| 17 | L6 | Strain gauges on inclinometer casing | 21.5 | |

*DEP* deep-earth probe, *DMS dielectric moisture sensor*

**Table 6** Sensors initially connected to the WSN

| Location | Piezometer depth (m) | Moisture sensor depth (m) | | Strain gauge depth (m) | | | | | | Geophone depth | Rain gauge height |
|---|---|---|---|---|---|---|---|---|---|---|---|
| | | 1 | 2 | 1 | 2 | 3 | 4 | 5 | 6 | | |
| L1 | 5.6 | 0.8 | 3.1 | 1.5 $x$ | 4.0 $x$ | 4.0 $\alpha$ | 7.0 $x$ | | | 5 cm | |
| L2 | 7.0 | 1.4 | | 3.0 $x$ | 3.0 $y$ | 6.0 $x$ | 6.0 $y$ | 9.0 $x$ | 9.0 $y$ | | |
| L3 | 15.6 | 1.0 | | 7.5 $x$ | 7.5 $y$ | 10.5 $x$ | 10.5 $y$ | 16.5 $x$ | 19.5 $x$ | | |
| L4 | 17.7 | 2.0 | | 3.5 $x$ | 3.5 $y$ | 6.5 $x$ | 9.5 $x$ | 11.5 $x$ | 11.5 $y$ | | |
| L5 | 14.0 | 0.6 | | 4.25 $x$ | 4.25 $y$ | 10.75 $x$ | 10.75 $\alpha$ | 10.75 $\beta$ | 15.0 $x$ | | 3 m |
| L6 | 14.3 | 2.0 | | 2.0 $x$ | 2.0 $y$ | 5.0 $x$ | 5.0 $y$ | 11.0 $x$ | 17.0 $x$ | | |

With reference to the strain gauge placement; $x$, $y$, $\alpha$, and $\beta$ refer to the direction along which the strain gauges measure movement as explained in the paper and depicted in Fig. 7

live to the internet. This real-time streaming of sensor data enables us to continuously monitor landslide activity in Anthoniar Colony, from anywhere around the globe. We then are able to report our findings to the government authorities and the local residents, thus promoting a feeling of security among the residents.

Data from the different sensors show a consistent pattern. The soil pore water pressures, as measured by the piezometers, increase after a particularly severe downpour or after periods of prolonged rainfall of moderate intensity and decrease as the rainfall decreases. The DMSs installed at *L1* (with the shallowest water table) show that the soil at this location is saturated through the main monsoon season, while DMSs at some of the other locations reflect some fluctuations in their readings immediately after a rain shower, indicating a temporary increase in the soil moisture content. The geophone has shown fairly constant readings since its installation during the pilot deployment.

Signals from the strain gauges show daily variations. These fluctuations can be attributed to corresponding variations in the temperature of the surrounding soil. However, after a heavy downpour, a few strain gauges, especially those at a depth of 10.75 m at *L5*, show significant signal variations. These fluctuations are most probably caused by some movement underneath the ground surface.

The most pronounced variations in strain gauge data were seen immediately after a severe downpour on 16 July 2009. Therefore, we present sensor data from the period 10 July 2009–9 August 2009 (Figs. 17, 18, 19, 20, 21, 22, and 23). The amount of rainfall was recorded every 24 h (Fig. 17), while data from the DEP sensors were sampled every 30 s and then averaged over a 6-h period to obtain the graphs shown in Figs. 18, 19, 20, 21, 22, and 23.

There was heavy rainfall in the state of Kerala during the month of July 2009, and many rainfall-triggered landslides occurred in this region. Daily rain data from Anthoniar Colony for the period 10 July–9 August 2009 are shown in Fig. 17.

In Fig. 18, data from the dielectric moisture sensors deployed at *L1*, *L2*, and *L4* are shown for the duration 10 July–9 August 2009. (Please note that the DMSs at *L3*, *L5*, and *L6* were connected to the WSN only after 9 August.)

Both the DMSs at *L1* show fairly constant readings throughout this period. We computed the degree of saturation of the soil using the DMS readings and the properties of the soil at *L1* (we have tested samples from this location in the laboratory). The readings from the DMS at the depth of 0.8 m indicated that during this period, the soil at *L1* (at the foot of the hill) was saturated at the fairly shallow depth of 0.8 m. As expected (please refer Table 2), the readings from the DMS at the depth of 3.1 m showed that the soil was saturated at this depth.

Thus, the two DMSs installed at *L1* show constant, saturated readings throughout the period shown in Fig. 18. The DMS installed at *L2* also shows fairly constant readings through most of this period.

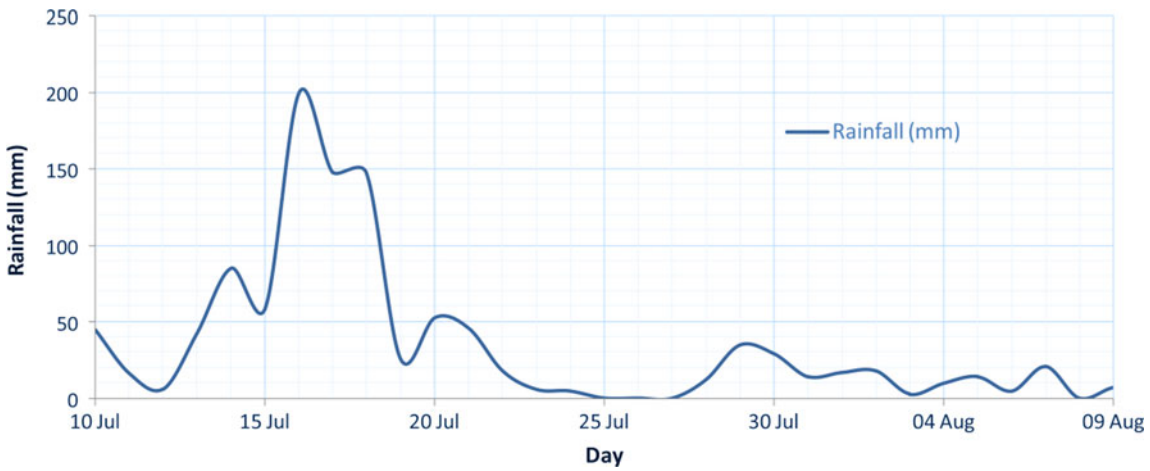


**Fig. 17** Anthoniar Colony rain data from 10 July 2009 to 9 August 2009

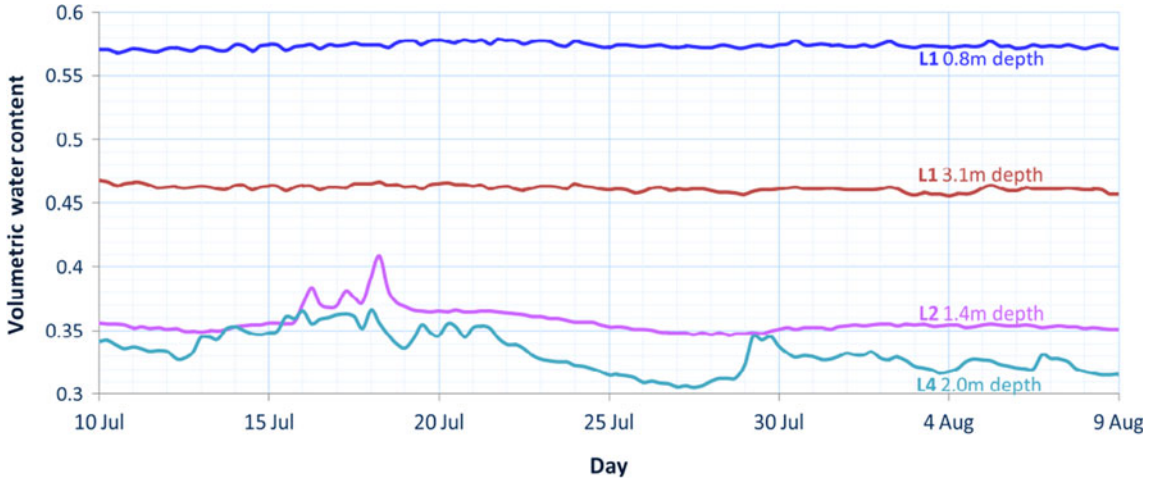


**Fig. 18** Dielectric moisture sensor data from 10 July 2009 to 9 August 2009

However, the DMS readings from *L2* do show sudden fluctuations immediately after a heavy downpour, such as the rainstorms on 16, 17, and 18 July.

In contrast, the DMS at *L4* does not show constant readings. Rather, the DMS readings, or the soil moisture content, increase immediately after a rain shower but decrease soon after. The position of *L4* may explain the continuous variations in the DMS readings. *L4* is near the crown of the hill and is at a substantially higher elevation than *L1* and *L2*. Rainwater drains away and thus the soil moisture does not attain a constant saturated value at a depth of 2.0 m.

There is a strong correlation between rainfall (Fig. 17) and the DMS data from *L4* (Fig. 18). Thus, we may be able to use DMSs installed in the higher regions of the hill to estimate rainwater infiltration rates.

Data from the piezometers at *L1*, *L2*, *L3*, *L4*, and *L5* are shown in Fig. 19. While the piezometer at *L3* was connected to the network only on 24 July, the piezometer at *L5* was disconnected from the network on 21 July for troubleshooting on the signal conditioning circuitries. The piezometer at *L6* was connected to the WSN only after the time period shown in Fig. 19.

As seen in Fig. 17, there was initially heavy rainfall in the month of July 2009, but the rainfall declined towards the end of the month. Therefore, as expected, we initially see an increase in pore water pressure, and then a decrease. Also as expected, we see the sharpest increase in pore pressure soon after the heavy downpour on 16 July. While all the piezometer data show the trend of increasing and then decreasing pore pressure, in our opinion, the most interesting data are shown by the piezometers at *L4* and *L5*.

The piezometer at *L5* is installed at a depth of 14.0 m. A steep increase in pore pressure occurs when the water level reaches 2.0 m above the piezometer. On studying our bore logs, we surmised that this steep increase in pore pressure may be attributed to a water level that reaches a soil layer with higher permeability above a soil layer of lower permeability. Our bore logs for *L5* record that the soil layer at depths of 9.8–11.7 m consists of sand with pebbles, while the layer immediately beneath consists of clay with silt and sand. Moreover, soil samples extracted from depths of 10.4–11.4 m had lower densities ($\sim 1.6\times10^3$ kg/m$^3$) than the average soil density at *L5* ($\sim 1.9\times10^3$ kg/m$^3$). Consequently, it is possible that this soil stratum has a higher void ratio as well as a higher permeability than the stratum just below. Interestingly, of all the strain gauges connected to our network, the *L5* strain gauges installed at depths of 10.75 m (that is, in the soil stratum discussed above) show the most pronounced signal fluctuations during periods of heavy rainfall.

The piezometer at *L4* shows the smallest increase in pore pressure. But *L4* is near the crown of the hill, and the water table is deepest at this

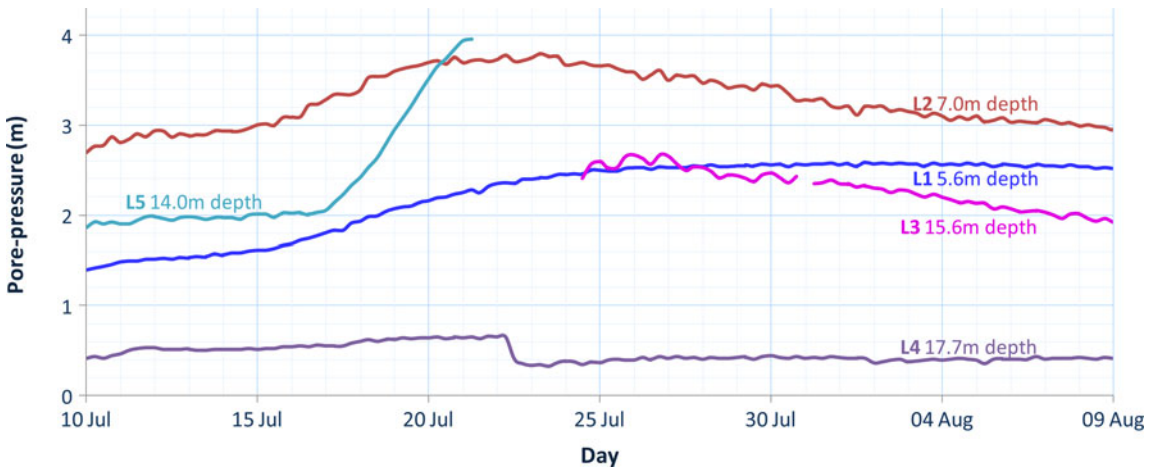


**Fig. 19** Piezometer data from 10 July 2009 to 9 August 2009

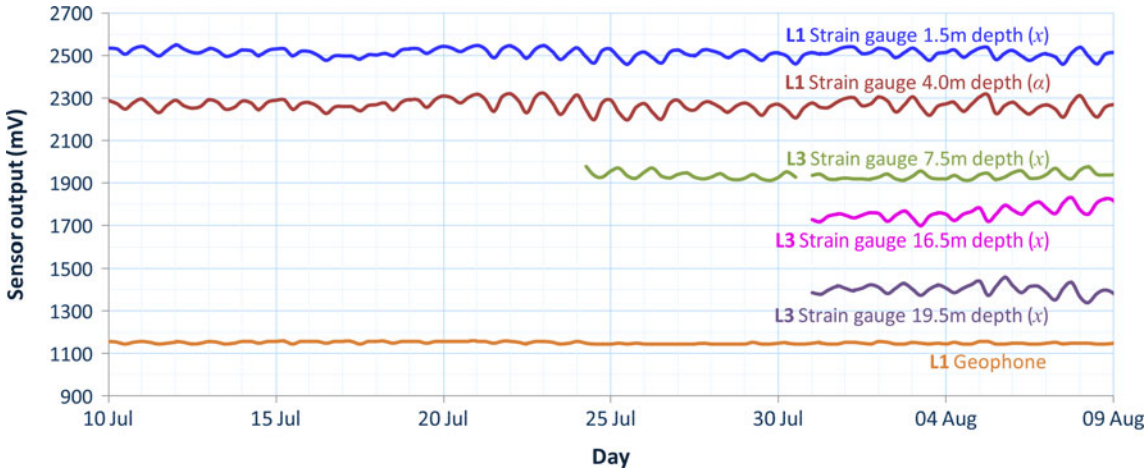


**Fig. 20** *L1* and *L3* strain gauge and geophone data from 10 July 2009 to 9 August 2009. In Figs. 20, 21, 22, and 23, the *alphabet in parenthesis* ($x$, $y$, $\alpha$, and $\beta$) refers to the direction along which the strain gauges detect motion as depicted in Fig. 7

location (Table 2). Rainwater has to percolate down a considerable depth to replenish the water table at this location, and it is expected that the increase and subsequent decrease in pore pressure will be least pronounced here.

The geophone installed at *L1* has shown fairly constant readings (Fig. 20) throughout its operation. These readings indicate the presence of only the usual ambient seismic noise and no unusual earth tremor activity in and around the landslide area.

Strain gauge data are shown in Figs. 20, 21, 22, and 23. Occasionally, signals from the strain gauges show a little disturbance immediately after the strain gauge is connected to the network, but for the most part, the signals only show a daily variation that can be attributed to changes in the temperatures of the surrounding soil.

However, the strain gauge data in Fig. 23 show significant signal fluctuations. These fluctuations begin on 16 July 2009, and they may indicate ground movement triggered by the downpours during the earlier part of that day.

The *L5* strain gauge 10.75 m($x$) shows the most significant signal fluctuations. The other strain gauges at a depth of 10.75 m also show noticeable signal variations, indicating movement that happened at a depth close to 10.75 m, and that movement presumably had a large component along the $x$-direction. Strain gauges 4.25 m($y$) and 15.0 m($x$) also indicate a slight movement, but strain gauge 4.25 m($x$) does not show any change in its readings.

The instabilities caused by these movements seem to have triggered further movement on 21 July, but probably in a different direction, as indicated by strain gauges 4.25 m($y$) and 10.75 m($\alpha$). Eventually, the strain gauges ceased to show unusual signal variations, possibly indicating that the slope had stabilized at that period of time.

## Conclusions

This paper describes the first major study on field instrumentation in the landslide-prone Western Ghats of India. This study convincingly demonstrates that it is possible to install a comprehensive wireless sensor network of deep-earth probes for landslide monitoring. Compared with earlier approaches, ours is the first full-scale WSN consisting of a variety of sensors—piezometers, dielectric moisture sensors, strain gauges, tiltmeters, a geophone, and a weather station—with some of these sensors installed at great depths.

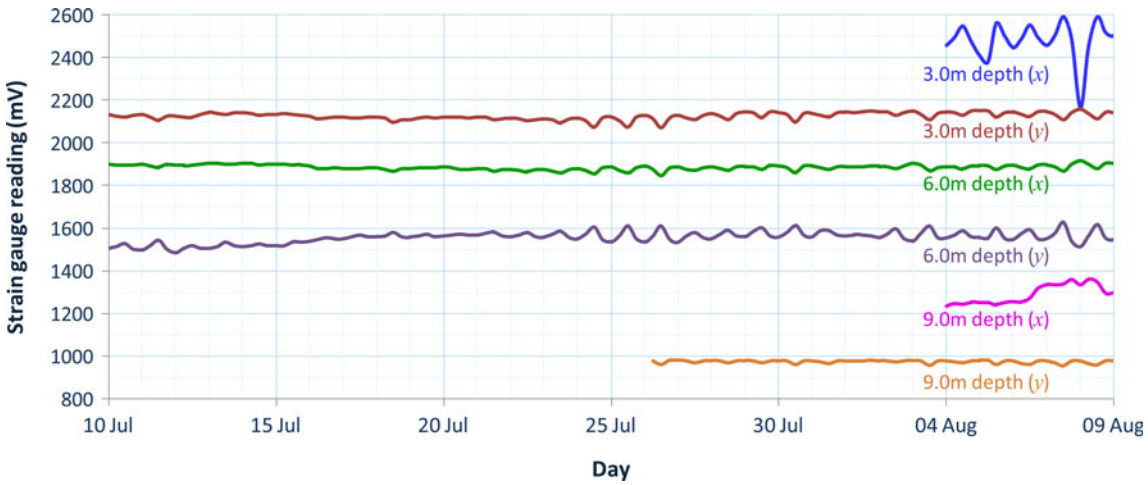


**Fig. 21** *L2* strain gauge data from 10 July 2009 to 9 August 2009

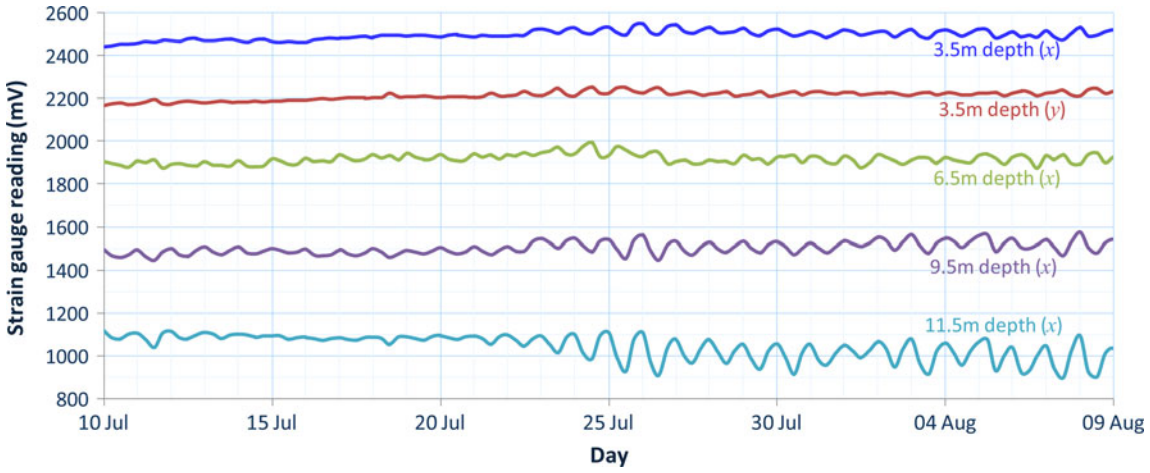


**Fig. 22** *L4* strain gauge data from 10 July 2009 to 9 August 2009

Our full-scale system has been in operation for more than 2 years; the deployment site is monitored remotely and in real time over the internet, demonstrating the value of a WSN for landslide monitoring. We have presented a description of the deployment site (in the Western Ghats of India) as well as some of the more interesting sensor data from the field deployment.

Data from some of the dielectric moisture sensors show a strong correlation with rainfall. However, as indicated in Fig. 18, DMSs installed at lower regions of the hill show fairly constant readings through the monsoon season, and thus we may not be able to use readings from these DMSs to estimate pore pressures. The piezometer data reaffirm the validity of the newer fully grouted method of piezometer installation, which is a faster, easier to install, and more fail-proof method.

Another important result of our study is that it shows that inexpensive instruments such as strain gauges and dielectric moisture sensors can be used successfully in landslide-monitoring networks. Strain gauges buried at great depths show signal variations indicative of slope movement. As part of our future work, we plan to derive a more precise quantitative relationship between these signal variations and actual slope movement.

Based upon this study, we believe that the future of WSNs for landslide monitoring is very promising, and the technology is likely to develop rapidly over the coming years. We expect that there will soon be newer wireless sensor nodes with improved memory and computational (data storage and processing) capabilities—thus, WSNs promise to become even more valuable tools in monitoring environmental phenomena.

## Acknowledgments

The authors gratefully acknowledge the help and cooperation that they have received from all their team members (all names listed in alphabetical order): Ms. Thushara Eranholi, Ms. Erica (Thapasya) S. Fernandes, Mr. Joshua (Udar) D. Freeman, Dr. H. M. Iyer, Mr. Sangeeth Kumar, Ms. Rekha P. Manoj, Mr. Prashant Omanakuttan, Mr. Manohar B. Patil, Mr. Mukundan T. Raman, Dr. Venkat P. Rangan, Mr. Vijayan Selvan, and Mr. Kalainger (Kailash) Thangaraju. We gratefully acknowledge Mr. Ranjith N. Sasidharan for preparing all the illustrations in this paper. And we thank Dr. Bharat Jayaraman, Ms. Karen (Sneha) Moawad, Mr. Anand Shenoy, and Ms. Vidhya Viswanathan for their help in preparing this paper.

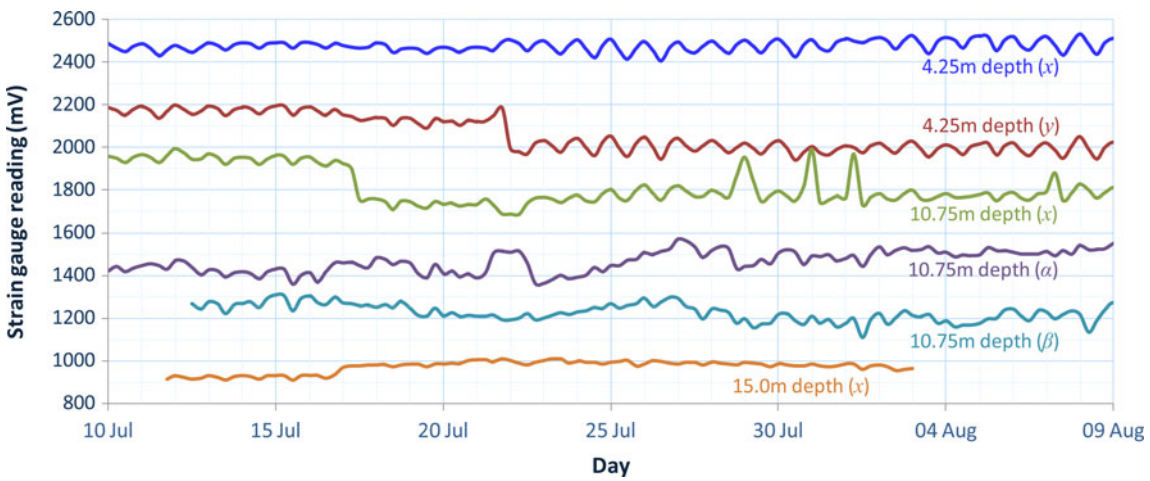


**Fig. 23** *L5* strain gauge data from 10 July 2009 to 9 August 2009

The soil tests were performed in the geotechnical laboratories of the Indian Institute of Technology (IIT)—Madras. We thank Dr. P. K. Aravindan for introducing us to the IIT faculty. We wish to express our gratitude to IIT professors Dr. Sailesh R. Gandhi and Dr. Retnamony G. Robinson and their students and technical staff—Mr. Sridhar Gangaputhiran, Ms. Nithya K. Maickam, Ms. Bushra S. Pareeth, Mr. Rakesh J. Pillai, Mr. Anburaj Radhakrishnan, Mr. Sam K. Sounderraj, Dr. Buvaneshwari Subramanian, and Mr. Saravanan T.—for all their help, support, and guidance in performing the laboratory tests.

We thank Dr. Raymond C. Wilson and Dr. Richard M. Iverson for all their timely and valuable advice and suggestions. We wish to express gratitude to all the field personnel who were involved in various capacities in this project. We thank the local residents and local administration of Anthoniar Colony for their help and cooperation during the deployment. We particularly wish to thank Mr. Mohan Irudhayadas and Mrs. Victoriya Suvithan, residents of Anthoniar Colony, for all their help throughout this project. And we thank the editor Dr. Matjaž Mikoš and the anonymous reviewers for reviewing the original manuscript with great care and providing valuable suggestions for its improvement.

Finally, words cannot express the immense debt of gratitude that we owe the Chancellor of our university, Sri. (Dr.) Mata Amritanandamayi Devi (Amma), for her involvement in our personal growth and guidance in all aspects of this project.

This work has been funded in part by the INFSO DG of the European Commission under the WINSOC (*Wi*reless Sensor *N*etworks with *S*elf-*O*rganizing *C*apabilities for critical and emergency applications) project, and in part by the Department of Information Technology (DIT) and the Department of Science and Technology (DST) of the Government of India.

## References

Acharya G, De Smedt F, Long NT (2006) Assessing landslide hazard in GIS: a case study from Rasuwa, Nepal. B Eng Geol Environ 65(1):99–107

Arnhardt C, Asch K, Azzam R, Bill R, Fernández-Steeger TM, Homfeld SD, Kallash A, Niemeyer F, Ritter H, Toloczyki M, Walter K (2007) Sensor based landslide early warning system-SLEWS. Development of a geoservice infrastructure as basis for early warning systems for landslides by integration of real-time sensors. In: Geotechnologien science report 10. Early warning systems in earth management. pp 75–88

Arnhardt C, Fernández-Steeger TM, Azzam R (2009) Monitoring of slope-instabilities and deformations with micro-electro-mechanical-systems (MEMS) in wireless ad-hoc sensor networks. Geophysical Research Abstracts 11: EGU2009-6048

Arnhardt C, Fernández-Steeger TM, Azzam R (2010) Sensor fusion of position- and micro-sensors (MEMS) integrated in a wireless sensor network for movement detection in landslide areas. Geophysical Research Abstracts 12: EGU2010-8828

Barr DJ, Swanston DN (1970) Measurement of soil creep in a shallow, slide-prone till soil. Am J Sci 269:467–480. doi:10.2475/ajs.269.5.467

Baum RL, McKenna JP, Godt JW, Harp EL, McMullen SR (2005) Hydrologic monitoring of landslide-prone coastal bluffs near Edmonds and Everett, Washington, 2001–2004. U.S. Geological Survey Open-File Report 2005–1063. p 42

Contreras IA, Grosser AT, Ver Strate RH (2008) The use of the fully-grouted method for piezometer installation. Geotechnical News 26(2):30–37

De Vleeschauwer C, De Smedt F (2002) Modeling slope stability using GIS on a regional scale. Proceedings of the First Geological Belgica International Meeting, Leuven, 11–15 September 2002. Aardkundige Mededelingen 12:253–256

Di Maio C, Vassallo R (2011) Geotechnical characterization of a landslide in a Blue Clay slope. Landslides 8(1):17–32

Fang Y, Lee B, King C, Chen M, Lien J, Yin H, Wang H (2008) Research on rainfall data of debris flow monitoring station via WSN technique and spatial analysis. American Geophysical Union, Fall Meeting 2008, Abstract H51F–0902

Fernández-Steeger TM, Arnhardt C, Walter K, Haß S, Niemeyer F, Nakaten B, Homfeld SD, Asch K, Azzam R, Bill R, Ritter H (2009) SLEWS—a prototype system for flexible real time monitoring of landslides using an open spatial data infrastructure and wireless sensor networks. In: Geotechnologien science report 13. Early warning systems in earth management. pp 3–15

Garich EA (2007) Wireless, automated monitoring for potential landslide hazards. Dissertation, Texas A&M University. p 56

Glabsch J, Heunecke O, Schuhbäck S (2009) Monitoring the Hornbergl landslide using a recently developed low cost GNSS sensor network. Journal of Applied Geodesy 3 (3):179–192

Grøneng G, Christiansen HH, Nilsen B, Blikra LH (2011) Meteorological effects on seasonal displacements of the Åknes rockslide, western Norway. Landslides 8(1):1–15

Hloupis G, Stavrakas I, Triantis D (2010) Landslide and flood warning system prototypes based on wireless sensor networks. Geophysical Research Abstracts 12: EGU2010-14166

Huang CC, Lo CL, Jang JS, Hwu K (2008) Internal soil moisture response to rainfall-induced slope failures and debris discharge. Engineering Geology 101(3–4):134–145

Iverson RM (2000) Landslide triggering by rain infiltration. Water Resources Research 36 (7):1897–1910

Jamaludin MZ, Aripin NM, Isa AM, Mohamed HWL, Alwee SMFS (2006) Wireless soil temperature and slope inclination sensors for slope monitoring system. Proceedings of the international conference on energy and environment (ICEE 2006), Kajang, Malaysia, 28–30 August 2006. p 5

Kim HW (2008) Development of wireless sensor node for landslide detection. Landslides and engineered slopes. From the past to the future. Proceedings of the tenth international symposium on landslides and engineered slopes, Xi'an, China, 30 June–4 July 2008. Edited by Chen Z, Zhang J, Li Z, Wu F, Ho K. pp 1183–1187

Kirschbaum DB, Adler R, Hong Y, Hill S, Lerner-Lam A (2010) A global landslide catalog for hazard applications: method, results, and limitations. Natural Hazards 52:561–575

Kuriakose SL, Jetten VG, Van Westen CJ, Sankar G, Van Beek LPH (2008) Pore water pressure as a trigger of shallow landslides in the Western Ghats of Kerala, India: some preliminary observations from an experimental catchment. Physical Geography 29(4):374–386

Kuriakose SL, Shankar G, Muraleedharan C (2009) History of landslide susceptibility and a chorology of landslide-prone areas in the Western Ghats of Kerala, India. Environmental Geology 57(7):1553–1568

Lee JMS (2009) Real-time monitoring of landslide using wireless sensor network. Dissertation, Ohio State University. p 201

Matsushi Y, Matsukura Y (2007) Rainfall thresholds for shallow landsliding derived from pressure-head monitoring: cases with permeable and impermeable bedrocks in Boso Peninsula, Japan. Earth Surf Process Landforms 32(9):1308–1322

McKenna GT (1995) Grouted-in installation of piezometers in boreholes. Canadian Geotechnical Journal 32(2):355–363

Mikkelsen PE, Green GE (2003) Piezometers in fully grouted boreholes. Symposium on field measurements in geomechanics, FMGM, Oslo, Norway, September 2003. p 10

Montgomery DR, Dietrich WE (1994) A physically based model for the topographic control on shallow landsliding. Water Resources Research 30 (4):1153–1171

Nadim F, Kjekstad O, Peduzzi P, Herold C, Jaedicke C (2006) Global landslide and avalanche hotspots. Landslides 3(2):159–173

Ochiai H, Okada Y, Furuya G, Okura Y, Matsui T, Sammori T, Terajima T, Sassa K (2004) A fluidized landslide on a natural slope by artificial rainfall. Landslides 1(3):211–219

Orense RP, Shimoma S, Maeda K, Towhata I (2004) Instrumented model slope failure due to water seepage. J Nat Disaster Sci 26(1):15–26

Petkovšek A, Fazarinc R, Kočevar M, Maček M, Majes B, Mikoš M (2011) The Stogovce landslide in SW Slovenia triggered during the September 2010 extreme rainfall event. Landslides. doi:10.1007/s10346-011-0270-z. p 8

Pinyol NM, Alonso EE, Corominas J, Moya J (2011) Canelles landslide—modelling rapid drawdown and fast potential sliding. Landslides. doi:10.1007/s10346-011-0264-x. p 19

Ramesh MV (2009) Real-time wireless sensor network for landslide detection. Proceedings of the third international conference on sensor technologies and applications, SENSORCOMM, Greece, 18–23 June 2009. pp 405–409

Ramesh MV, Raj R, Freeman J, Kumar S, Rangan PV (2007) Factors and approaches towards energy optimized wireless sensor networks to detect rainfall induced landslides. Proceedings of the 2007 international conference on wireless networks (ICWN 2007), Las Vegas, Nevada, U.S.A., 25–28 June 2007. Edited by Arabnia HR, Clincy VA, Yang LT. pp 435–438

Ray RL, Jacobs JM (2007) Relationship among remotely sensed soil moisture, precipitation and landslide events. Natural Hazards 43(2):211–222

Read RS, Langenberg W, Cruden D, Field M, Stewart R, Bland H, Chen Z, Froese CR, Cavers DS, Bidwell AK, Murray C, Anderson WS, Jones A, Chen J, McIntyre D, Kenway D, Bingham DK, Weir-Jones I, Seraphim J, Freeman J, Spratt D, Lamb M, Herd E, Martin D, McLellan P, Pana D (2005) Frank Slide a century later: the Turtle Mountain monitoring project. In: Hungr O, Fell R, Couture RR, Eberhardt (Eds.), Landslide Risk Management. Balkema, Rotterdam, pp 713–723

Rosi A, Mamei M, Zambonelli F, Manzalini A (2007) Landslide monitoring with sensor networks: a case for autonomic communication services. International conference on wireless technology for rural and emergency scenarios, IEEE CS, Roma, 2007. p 6

Rosso R, Rulli MC, Vannucchi G (2006) A physically based model for the hydrologic control on shallow landsliding. Water Resources Research 42:W06410. doi:10.1029/2005WR004369

Sattar A, Konagai K, Kiyota T, Ikeda T, Johansson J (2011) Measurement of debris mass changes and assessment of the dam-break flood potential of earthquake-triggered Hattian landslide dam. Landslides 8(2):171–182

Sheth A, Tejaswi K, Mehta P, Parekh C, Bansal R, Merchant SN, Singh TN, Desai UB, Thekkath CA, Toyama K (2005) Poster abstract—SENSLIDE: a sensor network based landslide prediction system. Proceedings of the third international conference on embedded networked sensor systems (SenSys 2005), San Diego, California, U.S.A., 2–4 November 2005. Edited by Redi J, Balakrishnan H, Zhao F. pp 280–281

Sheth A, Thekkath CA, Mehta P, Tejaswi K, Parekh C, Singh TN, Desai UB (2007) SENSLIDE: a distributed landslide prediction system. ACM SIGOPS Oper Syst Rev 41 (2):75–87

Shimoma S, Orense R, Honda T, Maeda K, Towhata I (2002) Model tests on slope failures caused by heavy rainfall. Int. Conference INTERPRAVEVENT 2002 in the Pacific Rim–Matsumoto, Japan. 2:547–557

Tahir AA, Ha SR (2011) Landslide hazard zoning along Himalayan Kaghan Valley of Pakistan—by integration of GPS, GIS, and remote sensing technology. Landslides. doi:10.1007/s10346-011-0260-1

Tang CJ, Dai MR (2010) Obtaining forewarning time for landslides using AMI associated wireless sensor network. Asia-Pacific Power and Energy Engineering Conference (APPEEC), Chengdu, China. 28–31 March 2010. pp 1–5

Terzis A, Anandarajah A, Moore K, Wang IJ (2006) Slip surface localization in wireless sensor networks for landslide prediction. Proceedings of the fifth international conference on information processing in sensor networks (IPSN 2006), Nashville, Tennessee, U.S.A., 19–21 April 2006. Edited by Stankovic JA, Gibbons PB, Wicker SB, Paradiso JA. pp 109–116

Tohari A, Nishigaki M, Komatsu M (2007) Laboratory rainfall-induced slope failure with moisture content measurement. J Geotech Geoenviron 133(5):575–587

Van Westen CJ, Terlien TJ (1996) An approach towards deterministic landslide hazard analysis in GIS: a case study from Manizales (Colombia). Earth Surf Proc Land 21 (9):853–868

Vařilová Z, Zvelebil J, Paluš M (2011) Complex system approach to interpretation of monitoring time series: two case histories from NW Bohemia. Landslides 8 (2):207–220

Williams PJ (1957) The direct recording of solifluction movements. American Journal of Science 255:705–715. doi:10.2475/ajs.255.10.705

Xinjian T, Dan Q, Tao S, Jun W, Xiangguo Y (2010) Monitoring bolt stress for cut slope based on wireless sensor network. Sixth international conference on wireless communications networking and mobile computing (WiCOM), Chengdu, China. pp 1–4

Yamada S, Kurashige Y (1996) Improvement of strain probe method for soil creep measurement. TJGU 17(1):29–38

Yin Y, Sun P, Zhang M, Li B (2011) Mechanism on apparent dip sliding of oblique inclined bedding rockslide at Jiweishan, Chongqing, China. Landslides 8 (1):49–65

**M. Ramesh · N. Vasudevan (✉)**
Amrita Center for Wireless Networks and Applications,
Amrita Vishwa Vidyapeetham (Amrita University),
Amritapuri, Kollam District, Kerala State, India
e-mail: nirmalav@am.amrita.edu

M. Ramesh
e-mail: maneesha@am.amrita.edu